ANOVA Investigation of Neural Network Guided Spurious Modes Reduction in Lithium Niobate MEMS Resonators

Ryan Tetro*, Luca Colombo*, Mary Beth Galanko-Klemash†, Sarah S. Bedair†, Ryan Rudy†, and Matteo Rinaldi*
*SMART Center, Northeastern University, Boston MA, USA
†US Army Research Lab, Adelphi MD, USA

***Abstract*—In this work, X-cut Lithium Niobate MEMS resonators are fabricated and tested to further identify and confirm the impact of design features on the rise of spurious modes. Building upon previous work, where a neural network identified the key features to be the number of electrode finger pairs, electrode length, and anchor width, 432 resonators were designed and fabricated to experimentally test and identify the contribution of these three features to spurious mode production. Each resonator had a unique combination of the design geometries spanning across three operating frequencies: 100 MHz, 200 MHz, and 400 MHz. By measuring the admittance and assigning a unique metric based on the severity of the spurious modes to each resonator, it was confirmed through analysis of variance (ANOVA) that each of the three design features and the frequency of operation have statistical significance in contributing to the rise of in-band spurious modes. Additionally, a linear regression model of the measured data concluded that the optimal Lithium Niobate resonator design to reduce the severity of in-band spurious modes requires a full anchor width, short aperture length, and a reduced number of IDE pairs. These results open the path to using advanced algorithms for further hardware optimization.**

***Index Terms*—MEMS, Neural Network, ANOVA, Lithium Niobate, Resonators**

I. Introduction

With the rapid advancement of 5G applications and the Internet of Things (IoT), there is an increasing demand for radio frequency (RF) piezoelectric microacoustic electromechanical systems (MEMS) that surpass the capabilities of current state-of-the-art devices [1] [2]. Key operational characteristics essential for applications like ultra-low-power wake-up receivers (WuRx) and tunable, reconfigurable filter banks include high quality factor (Q_s), high electromechanical coupling (k_t^2), impedance matching between the resonator static capacitance (C_0) and the load capacitance, and spurious-free response in the frequency range of implementation [3].

To achieve these desired properties and outperform commercially available Bulk Acoustic Wave (BAW) and Surface Acoustic Wave (SAW) resonators, various combinations of materials and modes, either fundamental or overtones, have been explored in recent years [4]. Among these technologies, noteworthy advancements have been made with Aluminum Nitride (AlN) and Scandium-doped Aluminum Nitride (ScAlN) Contour Mode Resonators (CMRs) [5] [6], Cross-sectional Lamé Mode Resonators (CLMRs) [7], Lead-zirconate Titanate (PZT) [8], quartz [9], and thin-film, single crystal Lithium Niobate (LN) resonators [10] [11] [12]. Notably, LN S_0 mode Laterally Vibrating Resonators (LVRs) have emerged as a promising acoustic technology, showcasing exceptional quality factors (up to 10,000 in vacuum) and large electromechanical coupling ($k_t^2 > 30\%$) at very and ultra-high frequencies (VHF/UHF) [13]. However, the combination of low intrinsic material losses and high piezoelectric coefficients renders this technology susceptible to undesired in-band spurious modes, which can detrimentally impact most envisioned applications [14]. Therefore, continued research in the design and optimization of resonators to mitigate the severity of in-band spurious modes is vital for future commercialization of this technology.

In previous work, a Neural Network (NN) aided design of LN resonators was executed to find the most significant contributors to in-band spurious modes [15]. By combining traditional analytical modeling [16], finite element analysis (FEA) [17], and Deep Feature Selection (DFS) within a NN framework [18], the ranking of design features contributing to spurious modes was achieved. The NN approach, aided by a spurious mode metric (M) based on the admittance response, highlighted the significance of three design features: the number of Interdigitated Electrode (IDE) finger pairs (N_p), the length of the aperture (L_e), and the width of the anchor (W_a). Although COMSOL® Multiphysics simulations confirmed that increasing N_p, decreasing L_e, and increasing W_a can reduce the spurious metric from M = 6 to M = 1 ($0 \leq M \leq 7$), experimental verification is still pending [15].

This paper aims to validate the findings from the NN approach and demonstrate an understanding of where spurious modes come from. Ultimately, this research aims to optimize LN resonators by identifying design parameters that effectively mitigate spurious modes. The first section of this work provides a brief overview of the resonators under investigation and their fabrication process. Additionally, a spurious mode metric (M) is introduced to quantify the severity of spurious modes. In the second section, the analysis of variance (ANOVA) method is discussed as a means to quantify the statistical significance of reducing spurious modes across various resonator design parameters. Finally, the third section presents the ANOVA and linear regression results, shedding light on the effective strategies for reducing spurious modes in LN resonators.

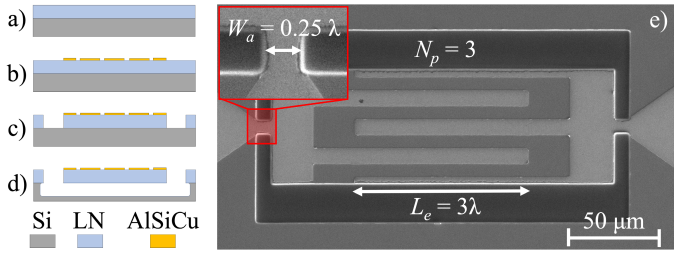

Fig. 1. Fabrication process for the LN resonators: a) Surface activated bonding and trimming to fabricate the thin film LN on silicon (performed by NGK); b) pattern the AlSiCu metal electrodes through the liftoff process; c) define the boundaries of the resonator plate using an ion mill etch; and d) release resonator plate in a XeF_2 etch. e) SEM image of a fabricated 100 MHz resonator with dimensions W_a = 0.25 λ, L_e = 3 λ, and N_p = 3.

II. Methods

A. Fabrication

The fabrication process of MEMS Laterally Vibrating Resonators (LVRs), as illustrated in Fig. 1 a-d, starts with a 1 µm (h) thin film X-cut 30° YZ Lithium Niobate (LN) on high-resistivity silicon wafer. First, metal traces are patterned on the top surface through the liftoff process. The photoresist (PR) is patterned with a direct write lithography tool, followed by 200 nm of sputtered Aluminum Silicon Copper (AlSiCu). The patterned PR is lifted off in a sonicated acetone bath, leaving behind the desired metal features on the top surface of the LN. These metal traces serve to electrically drive the resonator through the probing contact pads, which are connected to the resonator anchor, bus, and Interdigitated Electrodes (IDEs). The IDEs are spaced out by a half acoustic wavelength (λ), or pitch (p) to drive the S_0 mode, with a half width reflector at the resonator edge to satisfy the zero stress and maximum displacement boundary conditions [19].

To form the LN resonator plate, a second level of lithography and ion mill etch are employed. Once again, the PR is patterned using a direct write lithography tool to define the resonator plate boundaries and the anchor width. The exposed LN is then selectively etched down to the silicon substrate using an ion mill, precisely defining the rectangular boundaries of the resonator. Finally, the resonator plate is released from the supporting silicon substrate through an isotropic XeF_2 etch.

Each resonator is designed to have one unique combination of the four design variables displayed in Table I. An SEM image of a fabricated 100 MHz resonator is demonstrated in Fig. 1e with dimensions W_a = 0.25 λ, L_e = 3 λ, and N_p = 3. To evaluate the resonators' admittance frequency response, measurements are conducted using a VNA probe station equipped with GSG150 probes, calibrated with a SOLT calibration for the desired frequency range. Each resonator is individually probed to measure the admittance (Y_{12}) response around the designed resonant frequency, employing an appropriate IF bandwidth and a sufficient number of points to generate a detailed plot. The data for each resonator is saved as an .s2p file to be individually analyzed for the spurious modes present in the range of operation.

TABLE I
Design Variables

Variable	Symbol	Value
Finger Pairs	N_p	3 - 5 - 7 - 9 - 11 - 13
Aperture	L_e	3 – 5 – 7 – 9 – 11 – 13 λ
Anchor Width	W_a	0.25 – 0.5 – 1 λ
Frequency	f_s	100 MHz - 200 MHz - 400 MHz

B. Spurious Mode Metric (M)

In order to quantitatively assess the presence and severity of in-band spurious modes, a metric (M) is introduced in two different forms. For each device, the value of M is determined based on its Y_{12} response and the severity of the spurious modes observed. The first form of the metric, denoted as M_a, is assigned manually by analyzing the Y_{12} response and considering three factors: 1) peak cleanness, 2) number of in-band spurious modes, and 3) maximum spurious excursion (Δ_s). Based on these criteria, M_a can range from 0 to 7, and a complete list of the criteria can be found in Table II. An example of a measured device illustrating this metric is shown in Fig. 2. In this case, the device exhibits a clean peak (+0), three in-band spurious modes (+2), and a maximum spurious excursion between >5 dB and <20 dB (+1), resulting in a total metric value of M_a = 3.

The second form of the metric, denoted as M_b, is calculated by summing the excursions of each spurious mode (Δ_s) in dB directly from the Y_{12} data collected on the VNA. Following the approach outlined in [20], the in-band spurious mode peaks, as well as a small range of out-of-band peaks (to account for peak cleanness), are identified, and their individual excursions are summed using the following formula:

$$M_b = \sum_{j=1}^{n} |\max(Y_j) - \min(Y_j)| \tag{1}$$

Here, n represents the total number of spurious modes, and $\max(Y_j)$ and $\min(Y_j)$ correspond to the resonant and anti-resonant peaks of the j^{th} spurious mode, respectively. The process for identifying individual spurious mode peaks

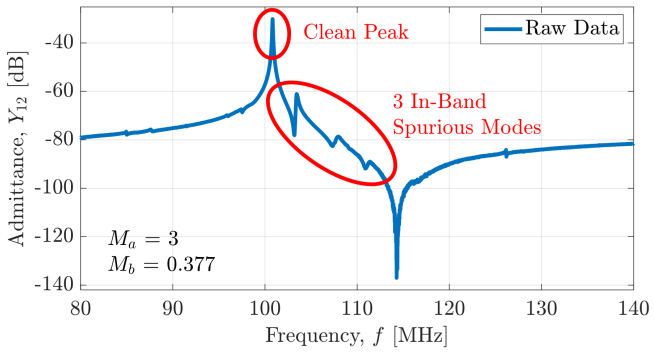

Fig. 2. Example admittance plot for a 100 MHz resonator with a clean resonant frequency peak (+0), 3 total in-band spurious modes (+2), and a maximum spurious excursion of >5 dB and <20 dB (+1), for a total of M_a = 3, according to [15]. Given the sum of the modes form [20], the resulting metric is M_b = 0.377.

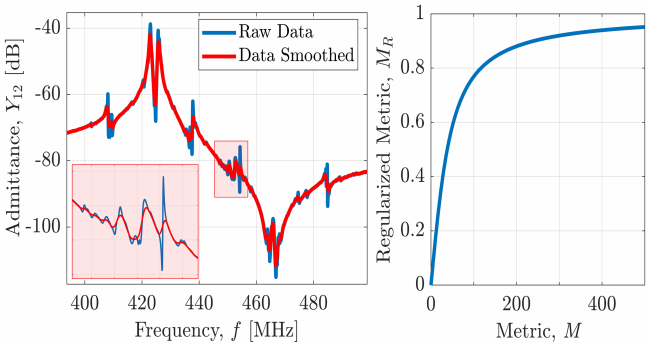

Fig. 3. a) Raw admittance (Y_{12}) plot for a 400 MHz resonator and the smoothed response. The data was smoothed with a binomial filter to remove small wiggles while still being able to identify the major peaks. b) Regularized metric (M_R) as a function of M, according to Eq. 2. The saturation function rescales M_b to constrain its value between 0 and 1.

TABLE II
SPURIOUS MODE METRIC CRITERIA

Factor	Criteria	Metric
Peak cleanness	Clean Peak	+0
	Disturbed Peak	+1
	Split Peak	+2
Number of in-band spurious modes	0	+0
	1 - 2	+1
	2 - 4	+2
	>4	+3
Maximum spurious excursion (Δ_s)	<5 dB	+0
	>5 & <20 dB	+1
	>20 dB	+2

starts with a smoothing operation, performed by a binomial filter, to remove any noise artifacts and ripples, as shown in Fig. 3a. Subsequently, a peak-finder operation is applied to the smoothed response to identify any spurious mode with a magnitude larger than 1 dB within the frequency range of interest. However, it should be noted that the smoothed data does not perfectly align with the raw data, as depicted in the inset of Fig.3a. To address this discrepancy, the approximate locations of the smoothed peaks are utilized to identify the corresponding peaks in the original data.

Given the nature of this metric, there is no upper bound for the size of M_b. Therefore, the complete set of metrics is regularized to be within a range of 0 and 1 using the following equation:

$$M_{R_i} = \frac{2}{\pi}\arctan\left(\frac{10}{M_{\text{max}}}M_i\right) \tag{2}$$

Here, M_i represents the metric for the i^{th} resonator, and M_{max} corresponds to the maximum measured metric across the entire dataset. The arctangent function serves as a saturation function [21], and therefore the resulting M_R is not an absolute metric, but successfully maps M_b to a value between 0 and 1, as shown in Fig. 3b. As a result, both metrics successfully quantify the severity of spurious modes, while offering the significant advantage of not relying on a priori knowledge of a spurious-free response [15].

C. Data Analysis

With each resonator having a unique combination of design variables (N_p, L_e, W_a, and f_s) and a resulting spurious mode metric (M), analysis of variance (ANOVA) is utilized to identify which variables have a statistically significant contribution to the production of spurious modes. ANOVA examines complex relationships between variables by partitioning the total variance of an observation into different sources. In this scenario, the observed variance is represented by the spurious mode metric, while the four design variables serve as the sources of variation. The ANOVA test compares the mean and variance of M for each design variable, and can conclude statistical significance in estimating M if there is a significant difference. This is visually demonstrated in Fig. 4, where histograms display the metric distribution for various anchor widths. By comparing and identifying significant differences in the variance and mean among the various anchor widths, ANOVA can determine statistical significance in estimating M when the anchor width is known.

Mathematically, ANOVA starts by calculating the variance between all the design variables (Fig. 4, All Resonators) and the variance within each design variable (Fig. 4, W_a = 0.25λ, 0.5λ, and 1λ). The standard equation of the variance is defined as:

$$s^2 = \frac{1}{n-1}\sum_{i=1}^{n}(M_i - \overline{M})^2 \tag{3}$$

where n represents the number of observations, M_i denotes the metric for the i^{th} resonator, and $\overline{M}$ is the mean of all the metrics. The denominator $n-1$ corresponds to the degrees of

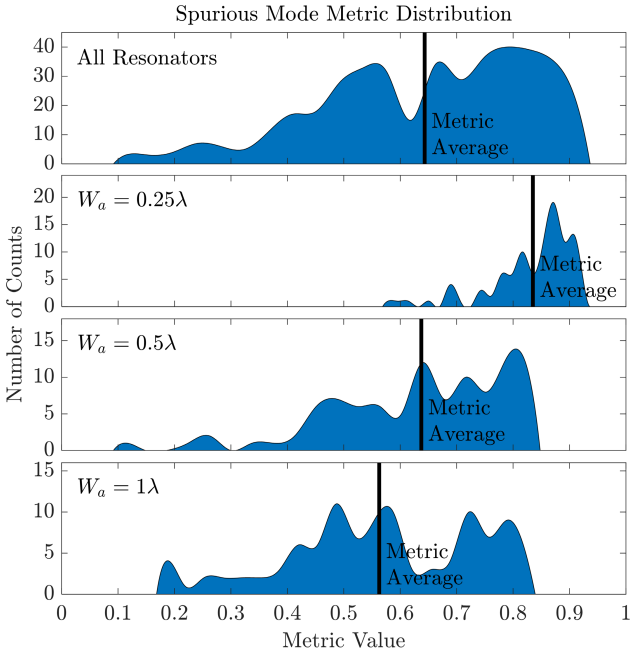

Fig. 4. Histogram depicting the spurious mode metric distribution for all resonators vs. resonators with various anchor widths. A visual representation of how ANOVA is able to conclude statistical significance in estimating M by comparing the mean and variance between each design variable.

TABLE III
ANOVA RESULTS - MANUAL SPURIOUS MODE METRIC FORM (M = 0 - 7)

Source	Sum Sq.	D.F.	Mean Sq.	F-Stat	P-Value
f_s	116.29	2	58.1449	120.94	0
W_a	96.184	2	48.0922	100.03	0
L_e	108.601	5	21.7202	45.18	0
N_p	20.698	5	4.1396	8.61	0

TABLE IV
ANOVA RESULTS - SUM OF THE MODES METRIC FORM (M = 0 - 1)

Source	Sum Sq.	D.F.	Mean Sq.	F-Stat	P-Value
f_s	0.9354	2	0.46769	66.04	0
W_a	5.1567	2	2.57833	364.09	0
L_e	1.5061	5	0.30122	42.54	0
N_p	0.6134	5	0.12269	17.32	0

freedom (D.F.), and the summation is referred to as the sum of squares (Sum Sq.), which collectively yield the mean square (Mean Sq.). The key to determining statistical significance is by calculating the F-Test Statistic (F), which is defined as the ratio of the variance between all the design variables and the variance within each design variable,

$$F = \frac{\text{Variance between design variables}}{\text{Variance within design variable}} = \frac{MS_{\text{variable}}}{MS_{\text{error}}} \quad (4)$$

From here, statistical significance is determined by calculating the probability (p-value) of F being larger than the observed value, The null hypothesis is rejected if the p-value is below some predefined significance level, such as $\alpha = 0.01$ for 99% confidence. If the null hypothesis is rejected, this suggests that the mean of one design variable is significantly different from the other design variables, indicating a direct impact on M.

Although ANOVA helps determine statistical significance, it does not provide insights into how each design variable contributes to in-band spurious modes. To assess the impact of each design variable on the severity of spurious modes, a linear regression model is employed with a normal distribution. This model generates a linear equation that estimates the value of M given the value of each design variable. The effect of each design variable is weighted by an estimated coefficient, where the sign and magnitude of these coefficients dictate how the value of M changes when a specific design variable is modified and the rest are held constant. The sign of the coefficient indicates a positive or negative correlation between M and the design variable, while the magnitude indicates how much M changes as the design variable is modified. These estimated coefficients serve as guidelines for optimizing resonator designs to reduce the severity of spurious modes.

III. MEASUREMENTS AND RESULTS

The ANOVA study conducted on the spurious mode metric for both approaches concluded that each design variable was statistically significant. The results depicted in Tables III and IV show that all the main factors have p-values equaling zero, implying that the null hypothesis is rejected and each factor correlates to the overall severity of spurious modes. These findings align with the insights gained from the Deep Feature Selection NN, thus validating our experimental observations. To further understand the impact of each design variable on the severity of in-band spurious modes, a linear regression model for a normal distribution is employed.

Upon examining the estimated coefficients in the linear models, Eq. 5 and 6, frequency exhibits the smallest effect on M with both positive and negative correlations. Considering the close to zero magnitudes, the impact of frequency on M is negligible for both metrics, leading to an inconclusive result. On the other hand, anchor width emerges as the most influential design variable, featuring the largest estimated coefficient with a negative correlation. This implies that increasing the anchor width will substantially reduce the value of M. The aperture length follows as the second most significant design variable with a positive correlation, suggesting that a shorter aperture length contributes to a reduction in spurious modes. Lastly, the number of finger pairs has a smaller estimated coefficient with a positive correlation, implying that utilizing fewer IDE finger pairs will slightly reduce the severity of spurious modes.

$$M_a = 3.45 - 0.0015f_s - 1.25W_a + 0.18L_e + 0.055N_p \quad (5)$$

$$M_b = 0.57 + 0.00023f_s - 0.33W_a + 0.020L_e + 0.011N_p \quad (6)$$

By incorporating interaction terms into the linear regression analysis, some general design guidelines can be inferred. Table V presents the estimated coefficients and p-values obtained from this analysis, highlighting the most significant design features as W_a, $W_a : L_e$, and $f_s : N_p$, which all have p-values ≈ 0. When examining the estimated coefficients of these three factors, again increasing the anchor width remains a key strategy for reducing the severity of in-band spurious modes. However, when considering the interaction with the aperture length, it becomes evident that increasing both the anchor width and aperture length leads to an increase in spurious modes. Therefore, a general design guideline emerges: increasing the anchor width while decreasing the aperture length, which agrees with linear models in Eq. 5 and 6. Lastly, while the interaction between f_s and N_p proves to be statistically significant, the estimated coefficient associated with it is exceedingly small. This finding reinforces our earlier conclusions that changes in frequency or the number of finger pairs have minimal impact on the generation of spurious modes.

In summary, the experimental results presented here validate the findings outlined by the neural network in [15]. The striking similarities observed in the results of both spurious mode metrics serve to confirm the effectiveness and reliability of the methods employed in this study. While the influence of frequency remains inconclusive due to its minimal effect, the anchor width stands out as the most impactful design variable in reducing M. Additionally, the aperture length and the number of finger pairs also contribute to reducing the severity of spurious modes, although to a lesser extent.

TABLE V
LINEAR REGRESSION RESULTS WITH INTERACTION TERMS - SUM OF THE MODES METRIC FORM (M = 0 - 1)

Source	Estimate	S.E.	T-Stat	P-Value
Intercept	0.86971	0.073543	11.826	6.7561e-28
f_s	-0.00043582	0.00019292	-2.2591	0.024411
W_a	-0.61322	0.071779	-8.5432	2.7354e-16
L_e	0.0045951	0.0066093	0.69524	0.48731
N_p	-0.0038644	0.0068735	-0.56222	0.57428
$f_s : W_a$	0.00037839	0.00014914	2.5372	0.01155
$f_s : L_e$	-1.7523e-5	1.4244e-5	-1.2302	0.21933
$W_a : L_e$	0.027599	0.005419	5.0931	5.4266e-7
$f_s : N_p$	6.9467e-5	1.425e-5	4.8748	1.571e-6
$W_a : N_p$	-0.0029051	0.0054463	-0.5334	0.59405
$L_e : N_p$	1.7726e-5	0.00052201	0.033957	0.97293

IV. CONCLUSION

Expanding upon the insights obtained from a NN, this paper experimentally tests and evaluates key LN resonator design features on the effect of in-band spurious modes. Utilizing the spurious mode metric (M), the NN identified anchor width, aperture length, and number of IDE finger pairs as the primary factors influencing spurious mode production. Though these findings were initially supported by FEA, this insight had yet to be tested experimentally. Therefore, 432 LN resonators were designed and fabricated, each incorporating a unique combination of the three design variables across three different frequencies. By measuring and quantifying the spurious mode metric (M) for each resonator, an ANOVA study was performed, confirming the statistical significance of each design variable in contributing to spurious mode production. A linear regression model was formulated to further understand the effect of each design variable and their interactions. This provided some general guidelines to reduce the number of in-band spurious modes and optimize the performance of LN resonators. It can be concluded that an optimal LN resonator design for mitigating spurious modes should feature a full anchor width, a shorter aperture length, and a reduced number of IDE finger pairs. While reducing spurious modes is a critical aspect in resonator design, other factors also influence the commercial success of LN resonators. This technique of utilizing neural networks to help aid the resonator design process can be extended to optimize quality factor, electromechanical coupling, and impedance matching, thus opening up avenues for further research and development.

ACKNOWLEDGMENTS

Research was sponsored by the Army Research Laboratory and was accomplished under Cooperative Agreement Number W911NF-19-2-0221. The views and conclusions contained in this document are those of the authors and should not be interpreted as representing the official policies, either expressed or implied, of the Army Research Laboratory or the U.S. Government. The U.S. Government is authorized to reproduce and distribute reprints for Government purposes notwithstanding any copyright notation herein.

REFERENCES

[1] R. Ruby, "A Snapshot in Time: The Future in Filters for Cell Phones," *IEEE Microwave Magazine*, vol. 16, pp. 46–59, Aug. 2015.

[2] Y. Yang, R. Lu, L. Gao, and S. Gong, "4.5 GHz Lithium Niobate MEMS Filters With 10% Fractional Bandwidth for 5G Front-Ends," *Journal of Microelectromechanical Systems*, vol. 28, pp. 575–577, Aug. 2019.

[3] L. Colombo, A. Kochhar, G. Vidal-Alvarez, and G. Piazza, "High-Figure-of-Merit X-Cut Lithium Niobate MEMS Resonators Operating Around 50 MHz for Large Passive Voltage Amplification in Radio Frequency Applications," *IEEE Transactions on Ultrasonics, Ferroelectrics, and Frequency Control*, vol. 67, pp. 1392–1402, July 2020.

[4] M. Kadota and S. Tanaka, "Improved quality factor of hetero acoustic layer (HAL) SAW resonator combining LiTaO3 thin plate and quartz substrate," in *2017 IEEE International Ultrasonics Symposium (IUS)*, (Washington, DC), pp. 1–4, IEEE, Sept. 2017.

[5] A. Lozzi, E. Ting-Ta Yen, P. Muralt, and L. G. Villanueva, "Al $_{0.83}$ Sc $_{0.17}$ N Contour-Mode Resonators With Electromechanical Coupling in Excess of 4.5%," *IEEE Transactions on Ultrasonics, Ferroelectrics, and Frequency Control*, vol. 66, pp. 146–153, Jan. 2019.

[6] S. Shao, Z. Luo, and T. Wu, "High Figure-of-Merit Lamb Wave Resonators Based on Al0.7Sc0.3N Thin Film," *IEEE Electron Device Letters*, vol. 42, pp. 1378–1381, Sept. 2021.

[7] C. Cassella, Y. Hui, Z. Qian, G. Hummel, and M. Rinaldi, "Aluminum Nitride Cross-Sectional Lamé Mode Resonators," *Journal of Microelectromechanical Systems*, vol. 25, pp. 275–285, Apr. 2016.

[8] S. S. Bedair, J. S. Pulskamp, R. Rudy, R. Polcawich, R. Cable, and L. Griffin, "Boosting MEMS Piezoelectric Transformer Figures of Merit via Architecture Optimization," *IEEE Electron Device Letters*, vol. 39, pp. 428–431, Mar. 2018.

[9] M. E. Galanko, S. S. Bedair, R. Rudy, V. F.-G. Tseng, J. S. Pulskamp, and I. Kierzewski, "AT-Cut Quartz Piezoelectric Transformers for Passive Voltage Gain in an RF Front-End," *IEEE Electron Device Letters*, vol. 40, pp. 1670–1673, Oct. 2019.

[10] R. Wang, S. A. Bhave, and K. Bhattacharjee, "High k_t^2xQ, multi-frequency lithium niobate resonators," in *2013 IEEE 26th International Conference on Micro Electro Mechanical Systems (MEMS)*, (Taipei, Taiwan), pp. 165–168, IEEE, Jan. 2013.

[11] R. Lu, T. Manzaneque, Y. Yang, and S. Gong, "Exploiting parallelism in resonators for large voltage gain in low power wake up radio front ends," in *2018 IEEE Micro Electro Mechanical Systems (MEMS)*, (Belfast), pp. 747–750, IEEE, Jan. 2018.

[12] M. Faizan and L. G. Villanueva, "Frequency-scalable fabrication process flow for lithium niobate based Lamb wave resonators," *Journal of Micromechanics and Microengineering*, vol. 30, p. 015008, Jan. 2020.

[13] R. Lu and S. Gong, "RF acoustic microsystems based on suspended lithium niobate thin films: advances and outlook," *Journal of Micromechanics and Microengineering*, vol. 31, p. 114001, Nov. 2021.

[14] L. Colombo, M. E. G. Klemash, T. M. Kiebala, S. S. Bedair, G. Piazza, and M. Rinaldi, "VHF and UHF Lithium Niobate MEMS Resonators Exceeding 30 dB of Passive Gain," *IEEE Electron Device Letters*, vol. 42, pp. 1853–1856, Dec. 2021.

[15] L. Colombo, L. Baldesi, T. Melodia, and M. Rinaldi, "Neural Network-Aided Spurious Modes Optimization Targeting Lithium Niobate MEMS Resonators," in *2022 IEEE/MTT-S International Microwave Symposium - IMS 2022*, (Denver, CO, USA), pp. 883–886, IEEE, June 2022.

[16] Y.-H. Song, R. Lu, and S. Gong, "Analysis and Removal of Spurious Response in SH0 Lithium Niobate MEMS Resonators," *IEEE Transactions on Electron Devices*, vol. 63, pp. 2066–2073, May 2016.

[17] C. Xu, E. Calayir, G. Piazza, M. Li, and S. Zhao, "Fast and accurate prediction of spurious modes in aluminum nitride MEMS resonators using artificial neural network algorithm," in *2017 IEEE International Ultrasonics Symposium (IUS)*, pp. 1–4, IEEE, Sept. 2017.

[18] T. M. Przytycka, ed., *Research in Computational Molecular Biology: 19th Annual International Conference, RECOMB 2015, Warsaw, Poland, April 12-15, 2015, Proceedings*. Springer International Publishing, 2015.

[19] L. Colombo, A. Kochhar, G. Vidal-Alvarez, P. Simeoni, U. Soysal, and G. Piazza, "Sub-GHz X-Cut Lithium Niobate *S0* Mode MEMS Resonators," *Journal of Microelectromechanical Systems*, vol. 31, pp. 888–900, Dec. 2022.

[20] L. Colombo, M. Ceran, and M. Rinaldi, "Spurious Modes Metric Definition for Machine Learning Aided MEMS Design," in *2022 IEEE International Ultrasonics Symposium (IUS)*, pp. 1–3, IEEE, Oct. 2022.

[21] D. Elliott, "A better activation function for artificial neural networks," 1993.